20 HELIOSEISMOLOGY II: probing the solar interior

In the last lecture, we showed that the wavefunction for solar p and f modes has the form

$$\Psi(r,\theta,\phi,t) \equiv \frac{P_1}{\sqrt{\rho}} = e^{-i\omega t} Y_{\ell m}(\theta,\phi)\hat{\psi}(r). \tag{1}$$

The frequency ω and radial wavefunction $\hat{\psi}$) satisfy

$$\frac{1}{r^2}\frac{d}{dr}\left(r^2\frac{d\hat{\psi}}{dr}\right) + \left[\frac{\omega^2 - U(r)}{v_s^2(r)} - \frac{\ell(\ell+1)}{r^2}\right]\hat{\psi} = 0, \tag{2}$$

in which

$$U(r) \equiv \frac{v_s^2}{r^2\sqrt{\rho}}\frac{d}{dr}\left(r^2\frac{d}{dr}\sqrt{\rho}\right). \tag{3}$$

Wherever the coefficient of $\hat{\psi}$ in (2) is positive and $\gg r^{-2}$, the solutions of this equation are oscillatory in r. They look locally like sines and cosines. Conversely, where the coefficient is negative, the solutions look like real exponentials that grow or decay with increasing r. In the former case, we can seek an approximate solution of the form

$$\hat{\psi}(r) \approx A(r)\exp\left(i\int^r k(r')dr'\right), \tag{4}$$

in which the radial wavenumber k and the envelope function A vary slowly with radius:

$$\frac{1}{A}\frac{dA}{dr} \sim \frac{1}{k}\frac{dk}{dr} \ll k(r). \tag{5}$$

Substituting (4) into (2) and dividing out the exponential factor yields

$$\left[\frac{\omega^2 - U(r)}{v_s^2(r)} - \frac{\ell(\ell+1)}{r^2} - k^2(r)\right] + \left[2ik\left(\frac{A'}{A} + \frac{1}{r} + \frac{k'}{2k}\right)\right] + \left[\frac{A''}{A} + \frac{2A'}{rA}\right] = 0. \tag{6}$$

The primes on k and A indicate derivatives with respect to r. Following (5), we assume that each set of terms in square brackets is smaller than the previous set by $\sim (kr)^{-1} \ll 1$.

To leading order we have

$$k^2(r) \approx \frac{\omega^2 - U(r)}{v_s^2(r)} - \frac{\ell(\ell+1)}{r^2}. \tag{7}$$

If the righthand side is positive, there are two real roots for k. The sign of each root determines the sign of the radial phase velocity, since

$$\text{Real}\left[\hat{\psi}(r)Y_{\ell m}(\theta,\phi)e^{-i\omega t}\right] \propto \cos\left(\omega t - \int^r k(r')dr' + m\phi + \varphi_0\right), \tag{8}$$

where φ_0 is a constant phase. Thus $k > 0$ corresponds to an outgoing wave. On the other hand, if the righthand side of (7) is negative, then both roots for k are imaginary, the argument of the exponential in (4) is real, and the solutions are *evanescent* rather than oscillatory. Regions where $k^2(r) < 0$ are called "forbidden" in quantum mechanics because the particle would be excluded from such regions classically, and its quantum-mechanical amplitude is exponentially small. Conversely, regions where $k^2(r) > 0$ are called "permitted."

Having determined $k^2(r)$, we equate the next set of brackets in (6) to zero to find A:

$$\frac{A'}{A} + \frac{1}{r} + \frac{k'}{2k} = 0 \implies A(r) = \frac{\text{const.}}{r|k(r)|^{1/2}}. \tag{9}$$

Since the absolute value of the exponential factor in (4) is constant in permitted regions, $|A(r)|$ describes how the envelope (=root-mean-square amplitude) of the wave varies with radius.

In general, the final set of brackets in (6) will not vanish, but these terms are small. WKBJ provides only an approximate solution, but often a very useful and accurate one. If desired, we could use these terms to compute higher-order corrections to k and A.

The inner and outer radii of the permitted region, r_- and and r_+ respectively, are determined by $k^2(r_\pm) = 0$ and are called *turning points*. An outgoing wave ($k > 0$) reflects from r_+ into an ingoing wave ($k < 0$). Similarly, an ingoing wave reflects from r_- into an outgoing one. In order to have a mode, it is necessary that the total phase change during a circuit from r_- to r_+ and back again should be a multiple of 2π; otherwise, the wave will interfere destructively with itself. Taking into account that in general each reflection introduces a phase shift (normally $\Delta\varphi = i\pi/2$ at a nonsingular turning point), we have

$$2\int_{r_-}^{r_+} |k(r)|dr \quad + \Delta\varphi_- + \Delta\varphi_+ = 2\pi n, \tag{10}$$

where n is a nonnegative integer, and the phase shifts $\Delta\varphi_\pm$ are (approximately) independent of ℓ and n. Since $k(r)$ depends on ω and ℓ through (7), the phase condition (10) determines ω in terms of ℓ and n.

The "potential" $U(r)$ is rather small compared to ω^2 except near the outer turning point $r_+ \approx R_\odot$, while the term $\ell(\ell+1)r^{-2}$ in (7) is relatively unimportant for $r > r_-$. Therefore, throughout most of the permitted region, $k^2 \approx (\omega/v_s)^2$. At this level of approximation, there is little point in worrying about the phase shifts $\Delta\varphi_\pm$, so that (10) can be cast in the very approximate form

$$2\int_{r_-}^{r_+} \frac{dr}{v_s(r)} \approx \frac{2\pi}{\omega} n. \tag{11}$$

The leftthand side is just what one would naively expect for the roundtrip travel time of a sound wave between the turning points. Thus, the equation says that this travel time should be an integral number of wave periods.

20.1 Overview of the data and principal results

Figure 1 is a dopplergram of the solar surface taken by the Michelson Doppler Imager (MDI) on board the Solar and Heliospheric Observatory spacecraft (SOHO). The grayscale is proportional to the line-of-sight velocity of the solar surface. The pattern you see is dominated by rotation, ~ 2 km s^{-1} at the limb on the equator. Loci of constant velocity would be parallel straight lines if the surface rotated rigidly, but the loci are curved because the sun rotates faster at the equator than at the poles. The smaller-scale structure in the velocity field is due mainly to convection (supergranulation) with a significant contribution from the incoherent sum of millions of modes.

After a geometric correction, the line-of-sight velocity can be converted to the radial component (v_r) with respect to coordinates centered on the sun, since the p-mode velocities are nearly radial at the surface. Then v_r can be decomposed into spherical harmonics:

$$v_r(r_\odot, \theta, \phi, t) = \sum_{\ell m} v_{\ell m}(t) Y_{\ell m}(\theta, \phi).$$

Note that the coefficients $a_{\ell m}$ can be determined as a function of time from a series of dopplergrams such as Fig. 1. These coefficients are then Fourier transformed:

$$\tilde{a}_{\ell m}(\nu) \equiv \int_{-T/2}^{T/2} a_{\ell m}(t) e^{2\pi i \nu t}\, dt, \tag{12}$$

where T is some long time interval (ideally, $T \to \infty$).[1] The square of the Fourier amplitude is the temporal power spectrum $P_{\ell m}(\nu) = |\tilde{a}_{\ell m}(\nu)|^2$, which has peaks at frequencies corresponding to global modes. Since the sun is nearly spherical and only slowly rotating, modes of the same degree ℓ and radial quantum number n have the same frequency $\nu_{\ell n} \equiv \omega_{\ell n}/2\pi$ and the same power regardless of the spherical-harmonic order m. Thus each panel of Fig. 2 shows the power spectrum for a given ℓ, and each peak corresponds to a particular n. At higher resolution, each of these peaks is split into a multiplet (with $2\ell + 1$ components in principle) corresponding to different m values. The splitting between different components of the same multiplet is caused by departures from spherical symmetry—mainly rotation.

One can plot the power spectrum two-dimensionally as a function of ℓ and ν, as in Fig. 3. The power is concentrated on curved ridges satisfying $\nu \propto \ell^{1/2}$ with different constants of proportionality. It can be shown (see below and the problem set) that each ridge corresponds to a separate n value. On a larger scale in this plot, one sees that the most strongly excited modes have frequencies in the range $2-5$ mHz, corresponding to periods of $3-8$ minutes, which explains why the observed

[1] We have written this transform in terms of the frequency $\nu = \omega/2\pi$: ν is measured in cycles per unit time (usually Hz= cycles/second), whereas ω is measured in radians per unit time.

p-modes were often referred to as the "five-minute oscillations." There appears also to be a trend with ℓ at fixed ν, but this is due partly to the way that the ridges crowd together at small ℓ. The fact that the mode amplitudes depend mainly upon ν rather than ℓ is a hint that excitation occurs mainly near the surface, because the high-(ℓ, n) eigenfunctions are all rather similar near their common outer turning point at $r_+ \approx R_\odot$, as one might deduce from (7).

Since the p-modes are basically resonant sound waves, one is not surprised to learn that their frequencies are sensitive to the sound speed as a function of position within the sun. Given enough of these modes, it is possible to invert for $v_s^2(r)$. This can now be done with such precision that one generally plots only the small differences between the inferred and predicted sound-speed profiles, the latter supplied by a theoretical solar model. Fig. 4 is such a plot ($c \equiv v_s$ not the speed of light!). Note the presence of horizontal as well as vertical error bars: with a finite number of modes, the inversion procedure gives the radial profile with limited radial resolution. Noise and measurement errors dominate the vertical error bars. Both kinds of error bar expand towards small radius because only the modes of lowest "angular momentum" ℓ penetrate the core, and there are relatively few such modes. Clearly, there are significant discrepancies between data and theory, especially just below the base of the convection zone, which occurs at $R_{\rm conv} \approx 0.71 R_\odot$. We still lack a fundamental quantitative theory for energy transport by turbulent convection. On the other hand, the discrepancies are significant only because the error bars are very small!

As mentioned earlier, frequency differences such as $\nu_{\ell,m,n} - \nu_{\ell,m',n}$ are sensitive to rotation and other departures from sphericity. These differences are small, but again because the data are excellent and the modes abundant, one is now able to measure the internal angular velocity of the sun rather well. Recent results are shown in Fig. 5. Notice that the angular velocity is roughly constant with radius but varies with latitude in the convection zone, while the core appears to rotate as a solid body. As we will see in the next lecture, the former presents a theoretical puzzle.

Finally, although large-scale and time-steady features such as the sound speed and rotation profiles are best measured from global mode frequencies, because these can be determined to high precision from long stretches of data, small-scale transient structures are better measured by entirely different methods more akin to terrestrial seismology [2]. The idea is to measure the *time of flight* τ_{PQ} between points P and Q on the solar surface; this can be accomplished by cross-correlating the radial velocities at these two points. Given an initial estimate of the sound-speed as a function of position below the surface, one can calculate the ray trajectories from P to Q and a first estimate of the time delay; deviations between the measured and observed delay are due to errors in the assumed sound speed field and to subsurface flows; given concurrent measurements between multiple pairs of points, one can invert for the temperature and flow-velocity fields below the surface. Recent results are shown in Fig. 6.

Let's look into the inversion problem in slightly more detail; for a thorough pedagogical treatment, see [4].

20.2 Determining the sound speed

The sound speed enters the the quantization condition (10) or (11) both explicitly, in the integrand, and implicitly, through the location of the turning points. Thus, the frequencies are sensitive to the run of v_s^2 with r. In fact, (11) implies the first-order variation in frequency $\nu = \omega/2\pi$ at a fixed

(ℓ, n) when $v_s \to v_s + \delta v_s$ is

$$\frac{\delta\nu}{\nu} \approx \int_{r_-}^{r_+} \frac{\delta v_s}{v_s^2}\, dr \Bigg/ \int_{r_-}^{r_+} \frac{dr}{v_s}\,. \tag{13}$$

(You might worry that the turning points $r_\pm$ themselves vary with $v_s(r)$. This is true. However, eq. (11) is only an approximation to the more accurate equation (10), whose integrand vanishes at the turning points, so that the contributions from the changes in $r_\pm$ vanish to first order.)

Given a sufficiently large number of accurately-determined frequencies, it is possible to reconstruct $v_s^2(r)$ and use it to test models of solar structure. Modes of high n but low ℓ penetrate most deeply and therefore are particularly important. In the past, one wanted urgently to constrain the central temperature of the Sun in order to isolate the cause of the solar neutrino problem [5]. Based on the good agreement between helioseismological inversions and stellar-structure theory, as demonstrated by Fig. 4, and from recent solar-neutrino experiments, especially [13], a consensus has emerged that the deficiency of ^8B neutrinos is not due to astrophysical errors but points to exotic neutrino physics.

20.3 The internal angular velocity

Another very important use of the helioseismological data is to determine the internal rotation of the Sun.

To study rotation, we have to go back to the derivation of the wave equation presented in the last lecture, and this time we must retain the most important terms involving the unperturbed velocity field $\vec{v}_0(\vec{r})$. For short-wavelength p-modes ($\lambda \ll R_\odot$), the largest terms involving $\vec{v}_0$ in the linearized equations are those accompanied by derivatives of the first-order quantities. Thus when we linearize $\vec{v}\cdot\vec{\nabla}\vec{v}$ in the Euler equation (4) [from the previous lecture], we keep $\vec{v}_0\cdot\vec{\nabla}\vec{v}_1$ but we ignore $\vec{v}_1\cdot\vec{\nabla}\vec{v}_0$, because the latter is smaller by $\sim \lambda/R_\odot$ than the former. When we linearize the continuity equation (5), we keep $\vec{v}_0\cdot\vec{\nabla}\rho_1$ but we discard $\rho_1\vec{\nabla}\cdot\vec{v}_0$—in fact a purely rotational velocity field satisfies $\vec{\nabla}\cdot\vec{v}_0 = 0$ anyway. As a result, the dominant effect of including the rotation is to convert

$$\frac{\partial}{\partial t} \to \frac{\partial}{\partial t} + \vec{v}_0\cdot\vec{\nabla} = \frac{\partial}{\partial t} + \Omega(r,\theta)\frac{\partial}{\partial\phi}. \tag{14}$$

Here $\Omega \equiv v_{\phi,0}/r/\sin\theta$ is the angular velocity. The operator on the right is the time derivative following the zeroth-order flow. Thus, inasmuch as the rotation enters the problem mainly through this operator, the physical interpretation is that the local dynamics of the p-modes is unaffected by (slow) rotation if we view the waves in a locally corotating frame.

Since Ω varies with $\vec{r}$, and since we analyze the mode frequencies in a nonrotating frame, the observed eigenfrequencies are affected by the rotation. For a mode with the $t\theta\phi$ dependence

$$e^{-i\omega t}Y_{\ell m}(\theta,\phi) \propto e^{-i\omega t + im\phi}P_\ell^m(\cos\theta), \tag{15}$$

the effect of the change in the operator (14) is to replace each ω in the 3D stationary-state wave equation (23) by $\omega - m\Omega$. This is closely analogous to a Doppler shift: wave frequencies change with a change in reference frame. If Ω were spatially constant, the resulting change in the eigenfrequencies

would be $\omega_{\ell mn} \to \omega^{(0)}_{\ell n} + m\Omega$, where $\omega^{(0)}_{\ell n}$ is the eigenfrequency computed without rotation. As Fig. 1 shows, however, Ω varies with θ on the surface. Thus the shift $\delta\omega$ caused by rotation has to be computed from some sort of spatial average of $m\Omega(r,\theta)$. The appropriate average is determined by a formalism similar to quantum-mechanical first-order perturbation theory:

$$\delta\omega_{\ell mn} \approx E^{-1}_{\ell mn} \int m\Omega(\vec{r}) \frac{|\psi_{\ell mn}(\vec{r})|^2}{2v_s^2(\vec{r})} dV. \tag{16}$$

Notice that volume elements are weighted by the energy per unit volume of the nonrotating mode, $|\psi_{\ell mn}|^2/2v_s^2$. The normalization factor out front is the reciprocal of the total energy,

$$E_{\ell mn} \equiv \int \frac{|\psi_{\ell mn}|^2}{2v_s^2} dV. \tag{17}$$

The frequency shifts caused by rotation are very small, on the level of 400×10^{-9}Hz ≈ 1 cycle per month: the solar equator rotates once in 27 days, as compared to a wave period ~ 5 min: thus

$$\frac{\delta\nu}{\nu} \sim \frac{5\,\mathrm{min}}{27\,days} \sim 10^{-4}.$$

This is smaller than the accuracy with which one can reliably compute the eigenfrequencies of a nonrotating sun, because of the residual uncertainties in its internal structure. (Note Figure 4 shows fractional descrepancies $\sim 10^{-3}$ between the measured and predicted sound speed.) In any nonrotating spherical model, however, modes of the same ℓ and n but different m would have exactly the same frequencies. Thus, reliable information about Ω can be obtained by studying frequency differences such as $\omega_{\ell,m+1,n} - \omega_{\ell,m,n}$.

Fig. 5 shows the result of inversion of such data to obtain $\Omega(R,\theta)$ for $0.2 \le r/R_\odot \le 0.85$ [1]. Notice that Ω is primarily a function of *latitude* ($= 90^\circ - \theta$) rather than radius in the convection zone, and that the rotation becomes uniform in the outer parts, at least, of the radiative core. (The inversion may not be reliable at the smallest radii shown. Better results can be expected from GONG datasets.) These results contradict a theorem to the effect that the angular velocity should depend only on cylindrical radius ($= r\sin\theta$) in regions where $\rho = \rho(P)$ [6]. We will prove this theorem next time. However, it makes assumptions that exclude magnetic fields, small latitudinal entropy gradients, and convective Reynolds stresses.

20.4 Excitation of the modes

What drives the modes?

The kappa mechanism, which drives radial pulsations of Cepheid and RR Lyrae variables, is one possibility. However, this mechanism is expected to be very weak in the Sun and probably overwhelmed by convective viscosity [7]. Also, the kappa mechanism normally drives modes with frequencies $\lesssim (G\bar{\rho})^{1/2}/2\pi$, which is about 100μHz in the solar case. As shown by Figures 4 and 10, the most strongly excited helioseismic modes have $\nu \sim 3000\mu$Hz. Still another objection to the kappa mechanism is that they should not be able to excite the high-ℓ f modes at all, because these modes (like ocean surface waves) do not perturb the density, temperature, or opacity of fluid

elements. Yet the f modes ($n = 0$) are observed to be excited to amplitudes comparable to those of the p modes ($n > 0$) at comparable frequencies.

The presently preferred theory is that the modes are stochastically driven by turbulent convection in the outermost parts of the convection zone [7, 8, 9]. This is somewhat analogous to the emission of sound by water boiling on your stove (except that bubbles may play a dominant role in that case, especially at the higher frequencies); the theory of emission of sound by nearly-incompressible turbulence was pioneered by the British mathematical physicist Lighthill [12] The pressure fluctuations associated with the turbulence couple to sound waves. The coupling is a very strong function of the turbulent Mach number $\mathcal{M} \equiv v_{\rm conv}/v_s$. Large slow eddies at depth are extremely subsonic and are very inefficient emitters. The small rapid ones near the surface, which have correlation times of a few minutes, dominate. Because the excitation occurs so close to the surface, it is almost independent of ℓ, since for all the resolvable modes $kR_\odot \gg \ell$ near the photosphere.

References

[1] `http://sohowww.nascom.nasa.gov/gallery/MDI/`

[2] Duvall, T. L. Jr., Jefferies, S. M., Harvey, J. W., & Pomerantz, M. A., 1993, Nature, 362, 430.

[3] Duvall, T. L. Jr., et al. 1997, Solar Physics, 170, 63.

[4] Christensen-Daalsgard, J. 1998, Lecture Notes on Stellar Oscillations `http://www.obs.aau.dk/~jcd/oscilnotes/`

[5] Bahcall, J.N. 1989, Neutrino Astrophysics, (New York: Cambridge U. Press).

[6] Tassoul, J.-L. 1978, Theory of Rotating Stars, (Princeton: Princeton U. Press), §4.3

[7] Goldreich, P. & Keeley, D. 1977, ApJ 211, 934; *ibid* 212, 243.

[8] Goldreich, P. & Kumar, P. ApJ 326, 462

[9] Goldreich, P., Murray, N. & Kumar, P. ApJ 424, 466

[10] Kosovichev, A. G. et al., 1997a, in IAU Symp. 181, Sounding Solar and Stellar Interiors, p. 203

[11] Kosovichev, A. G. et al., 1997b, Solar Physics, 170, 43

[12] Lighthill, J. 1952, Proc. Roy. Soc. A, 211, 564.

[13] Sudbury Neutrino Observatory: `www.sno.phy.queensu.ca`.

Figure 1: Doppler image of the solar disk, taken by the Michelson Doppler Imager on board the Solar and Heliospheric Observatory [1].

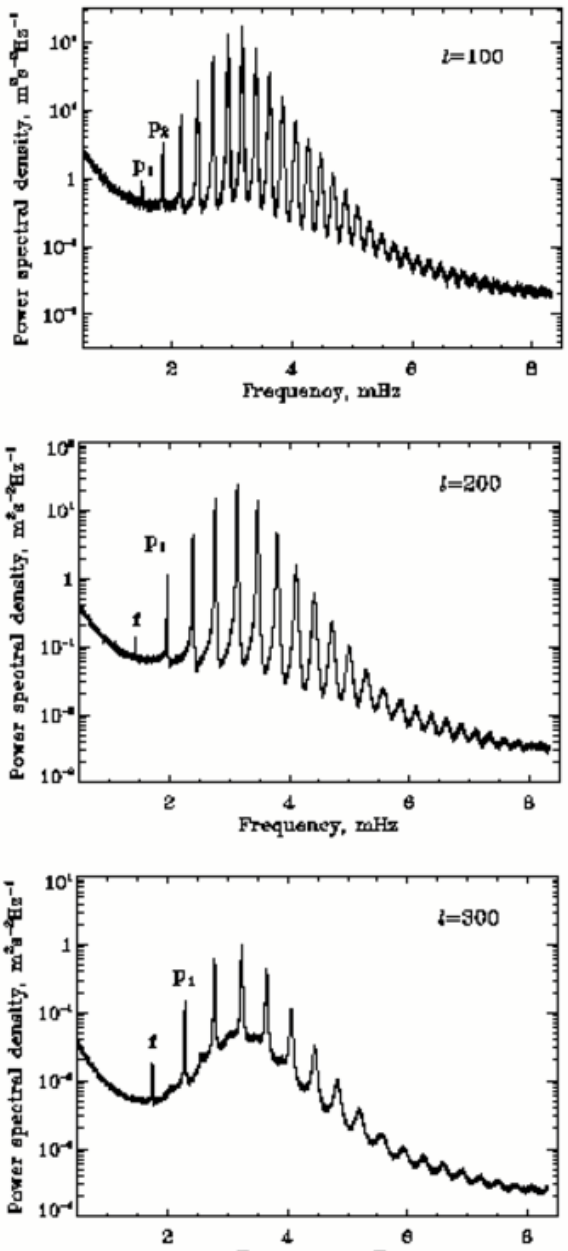

Figure 2: Temporal power spectra from MDI/SOHO at selected values of spherical-harmonic degree l [1]. Note 3.33 mHz = 1 cycle/(5 min).

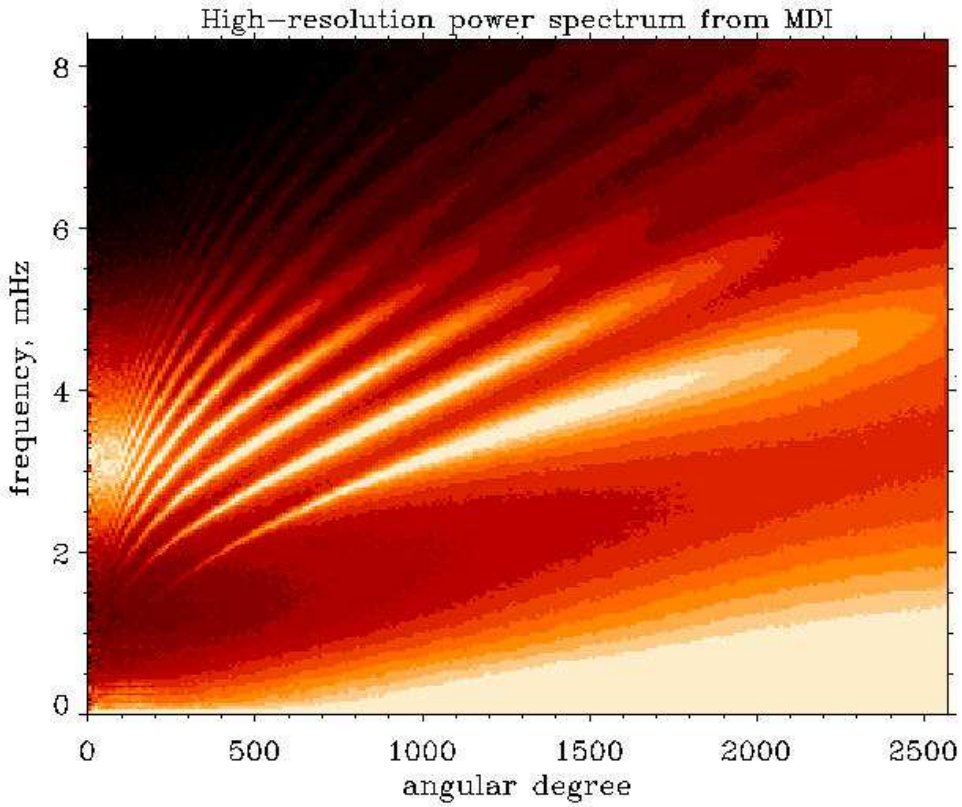

Figure 3: Observed power vs. frequency and l. Each ridge line corresponds to a particular n. [1].

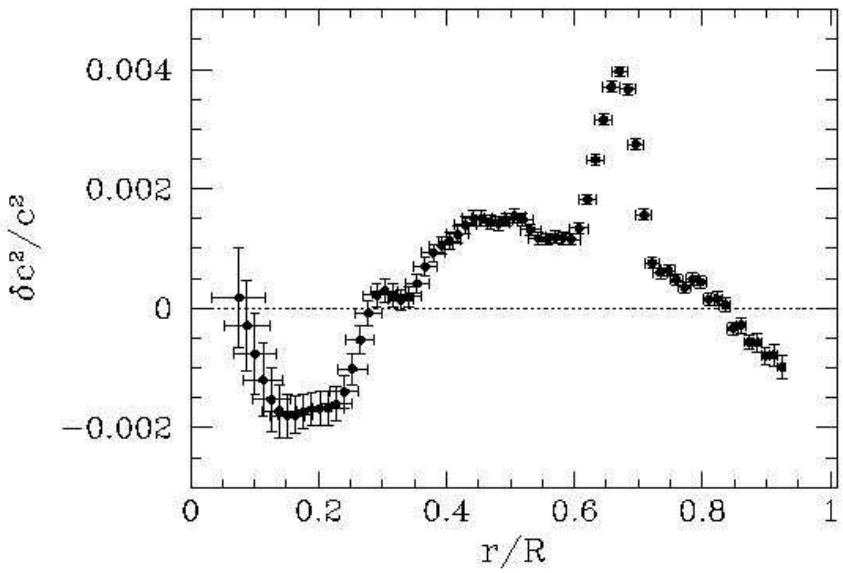

Figure 4: Deviations between sound speed predicted by solar model and sound speed by inversion of helioseismological data [1, 10].

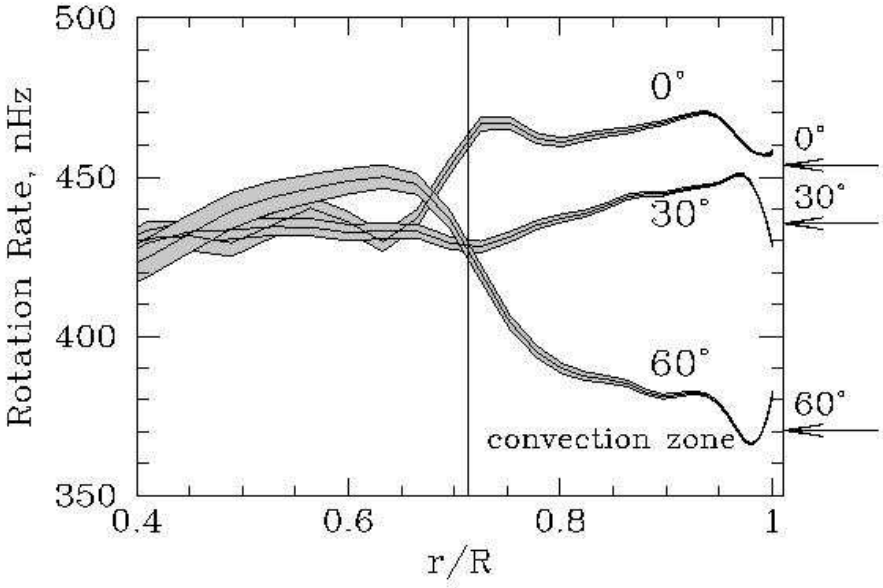

Figure 5: Internal angular velocity at three solar latitudes[1, 11]. Note: 400 nHz = 1 cycle/(30 d).

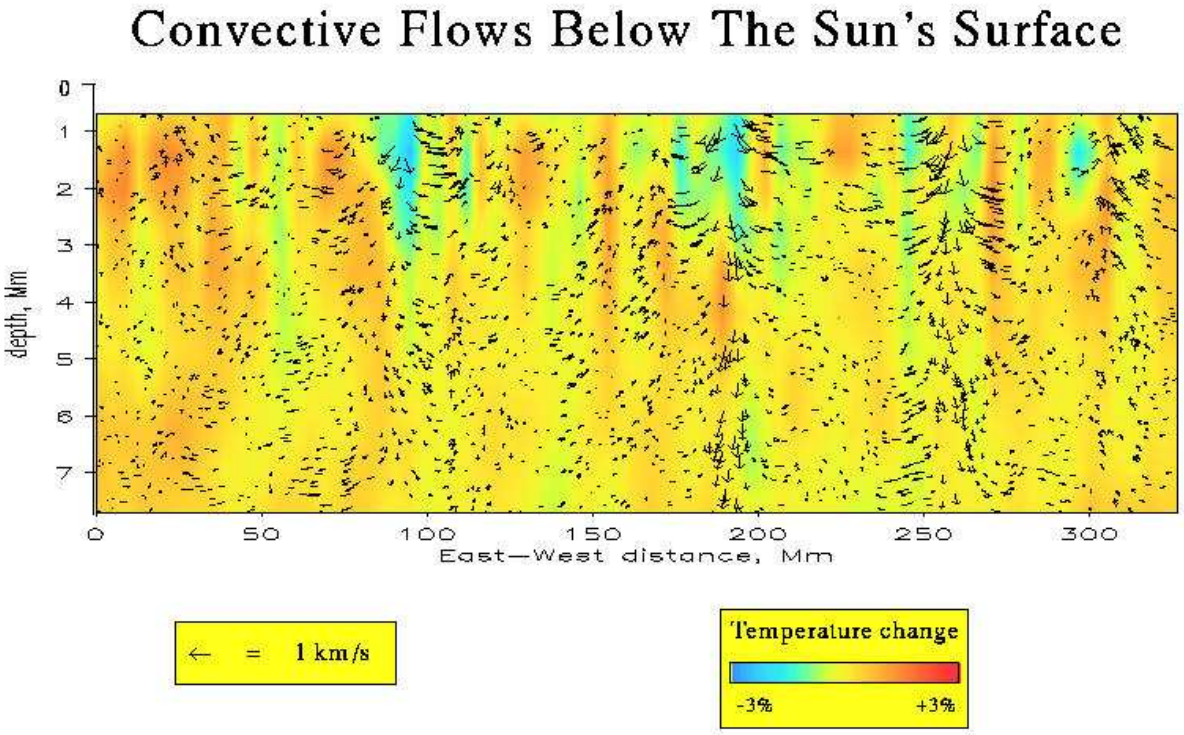

Figure 6: Convection below the solar surface imaged by time-distance helioseismology.[1, 3]